

# Development of stereoscopic molecular tagging velocimetry

D. G. Bohl, M. M. Koochesfahani, B. J. Olson

302

**Abstract** This paper describes the development of a stereoscopic molecular tagging velocimetry (sMTV) technique for measuring the instantaneous three-component velocity field over a plane in a flow. The calibration technique employed allows the stereo imaging parameters to be determined directly from a target image without the direct physical measurement of those parameters. Effects of index of refraction variations are accounted for approximately in the calibration method. Sensitivity analysis and target test experiments for a typical optical setup indicate maximum error levels for the in-plane components to be nominally the same as two-component MTV measurements. The error in the out-of-plane velocity component can be one to three times larger, depending on the stereo viewing angle. Experimental results are presented to validate the sMTV technique against other known measured results, along with an application to the highly three-dimensional flow field near the tip of a model propeller.

## 1 Introduction

Molecular tagging velocimetry (MTV) is a whole field optical technique which relies on molecules that can be turned into long lifetime tracers upon excitation by photons of an appropriate wavelength. Typically a pulsed laser is used to “tag” the regions of interest, and those tagged regions are interrogated at two successive times within the lifetime of the tracer. The measured Lagrangian displacement vector provides the estimate of the velocity vector. This technique can be thought of as essentially a *molecular* counterpart of particle image velocimetry (PIV), and complements it where the use of seed particles is not desirable difficult or may lead to complications. In our

implementation of MTV, typically a grid of intersecting laser lines is used for tagging purposes and a spatial correlation method is utilized to determine the displacement of the tagged regions. An example of an MTV image pair and the resulting velocity field are shown in Fig. 1 for the flow of a vortex ring approaching a solid wall at normal incidence. Detailed discussions of the planar MTV technique can be found in Koochesfahani et al. (1996), Gendrich and Koochesfahani (1996), Gendrich et al. (1997) and Koochesfahani (1999).

Past applications of MTV have considered the measurement of either one or two components of the velocity vector over a plane. Accurate results can be obtained in these applications as long as the flow field is either uni-directional or two-dimensional, respectively. As is also encountered in other optical imaging techniques such as PIV, the out-of-plane motion in a highly three-dimensional flow can seriously impact the accuracy of the in-plane velocity measurements; see for example Prasad and Adrian (1993). While these effects can be minimized by the appropriate choice of optics the better approach is to attempt to measure all three components of the velocity vector. This approach offers the clear advantage of also providing a more complete picture of the flow field. The work described here reports the development and performance characteristics of a stereoscopic molecular tagging velocimetry (sMTV) technique.

## 2 Technique development

The stereo imaging approach is commonly used in the field of machine vision and also in PIV to obtain the three components of the displacement field. Two basic approaches, lens translation and angular displacement have been utilized for this purpose. In the lens translation method, two detectors are placed side by side with the image plane parallel to the object plane. Detailed discussion of this method can be found in Arroyo and Greated (1991), Gauthier and Riethmuller (1988), Prasad and Adrian (1993) and Solof et al. (1997). The work described here takes advantage of the angular displacement method; see the schematic in Fig. 2. In this approach, two cameras view the same region of interest from an angle, and the image planes are rotated with respect to the object plane. The nearly entire overlap between the two images in this configuration is the motivating factor for use of this method. Note that the lens translation method can also be configured to provide nearly complete overlap; however,

Received: 20 December 1999/Accepted: 8 May 2000

D. G. Bohl, M. M. Koochesfahani, B. J. Olson  
Department of Mechanical Engineering  
Michigan State University, East Lansing, MI 48824, USA

Correspondence to: D. G. Bohl

This work was supported by the MRSEC Program of the National Science Foundation, Award Numbers DMR-9400417, and DMR-9809688. We gratefully acknowledge Dr. Richard Cohn's contributions to the initial developments of the work described here.

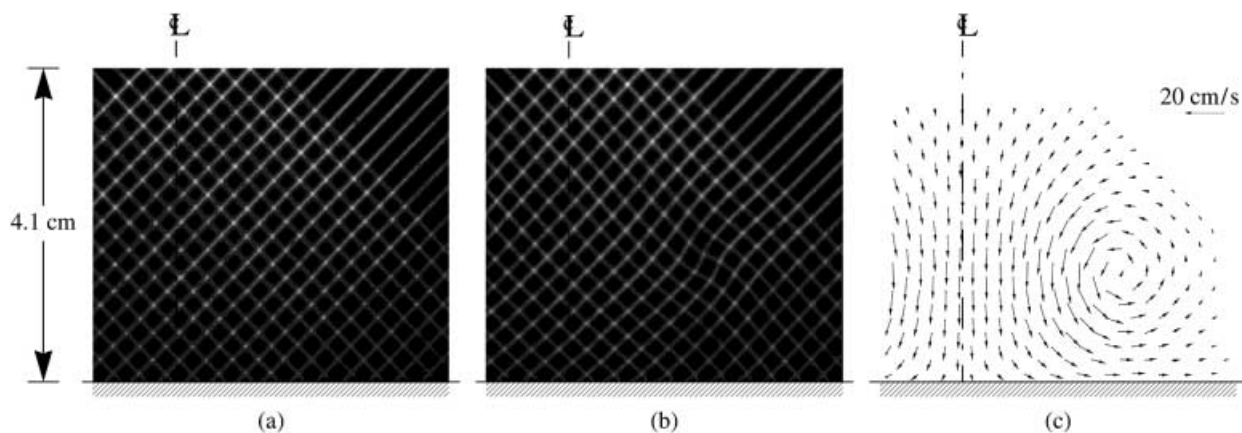


Fig. 1a-c. Typical MTV image pairs and the resultant two-component velocity vector field (Gendrich et al. 1997). The flow shown is from a vortex ring impacting a flat wall at normal

incidence. The axis of symmetry is indicated by the dashed lines: a grid imaged 1  $\mu$ s after the laser pulse; b same grid imaged 8 ms later; c velocity field derived from a and b

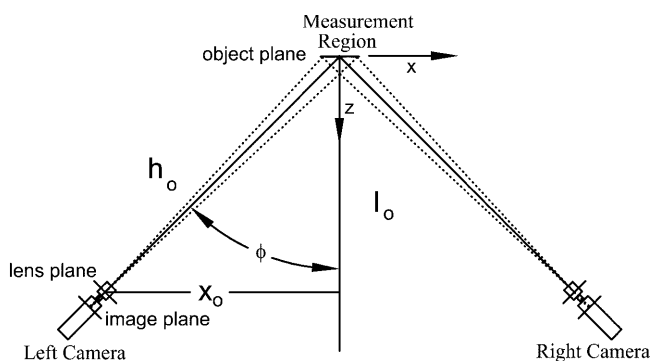


Fig. 2. Schematic of angular displacement stereoscopic method. Distances and angles are derived independently for each camera

additional optical distortions are introduced that must be accounted for (Prasad and Adrian 1993; Solof et al. 1997).

The angular displacement method generally leads to two disadvantages. The first disadvantage is that a finite depth of field leads to non-uniform focus over the viewed area. The second disadvantage occurs when viewing image planes through media with varying indices of refraction. The total internal reflection angle sets a limit on the permissible viewing angle for the detectors, which may be less than optimum for stereoscopy. Methods for overcoming the total reflection issue (e.g., liquid prisms) and the depth of field issue (e.g., utilizing the Scheimpflug condition) have been developed; see van Oord (1998) and Hill et al. (1999). However, these solutions preclude the use of simple geometric relationships. For further discussion of the angular method see also Gauthier and Riethmuller (1988), Westerweel and Nieuwstadt (1991), Lawson and Wu (1997b) and Willert (1997). It should be mentioned that the non-uniform focus related to finite depth of field in the angular displacement method does not bring a major disadvantage to MTV applications. Here, only the tagged region is luminescent and correlates uniquely with the same region displaced by the flow, as long as the displaced region is still in the field of view.

Following along geometric arguments similar to those by Westerweel and Nieuwstadt (1991) and Gauthier and Riethmuller (1988), we have developed the equations for extracting the three components of the velocity from the apparent two-component velocity data obtained from the two detectors. The current equations are more general, however, in that they do not assume identical imaging parameters between the two cameras, removing this restriction. Using a two-step process, the displacement field from each detector is first re-mapped independently from the detector's image plane (pixel space) to the object plane (real space) followed by combining these apparent in-plane displacements to obtain the actual three components of the displacement field.

The equations used for remapping the coordinates  $(x'', y'')$  on the detector's image plane (pixel space) to  $(x, y)$  on the object plane (real space) are given by

$x$ -component:

$$x_l = \frac{h_{o,l} m_l x_l''}{h_{o,l} \cos \phi_l - m_l x_l'' \sin \phi_l} \quad (1)$$

$$x_r = \frac{h_{o,r} m_r x_r''}{h_{o,r} \cos \phi_r + m_r x_r'' \sin \phi_r}$$

$y$ -component:

$$y_l = m_l y_l'' \left( 1 + \frac{x_l \sin \phi_l}{h_{o,l}} \right) \quad y_r = m_r y_r'' \left( 1 - \frac{x_r \sin \phi_r}{h_{o,r}} \right) \quad (2)$$

In these equations, the subscripts l and r refer to the left and right cameras, respectively. The remapping equations are arrived at by first transforming the image plane to a rotated "virtual object plane" parallel with the image plane, and then projecting this plane onto the real object plane. The derivation assumes that the magnification  $m$  is uniform, where  $m$  is defined as the image ratio of the virtual object plane to the image plane.

The actual  $x$ ,  $y$  and  $z$  displacements are found by combining the apparent in-plane displacements from the two detectors according to the following relations:

$$dx = \frac{l_{o,r}(x_r - x_{o,r})(x_{o,l} + x_l + dx_l) - l_{o,l}(x_l + x_{o,l})(-x_{o,r} + x_r + dx_r) + (l_{o,r} - l_{o,l})(x_{o,l} + x_l + dx_l)(x_{o,r} - x_r - dx_r)}{-[l_{o,l}(x_{o,r} - x_r - dx_r) + l_{o,r}(x_{o,l} + x_l + dx_l)]} \quad (3a)$$

$$dy = \frac{(y_l + dy_l)(y_r + dy_r)(x_{o,r} + x_{o,l} + x_l - x_r) - y_l(y_r + dy_r)(x_{o,l} + x_l + dx_l) - y_r(y_l + dy_l)(x_{o,r} - x_r - dx_r)}{(y_r + dy_r)(x_{o,l} + x_l + dx_l) + (y_l + dy_l)(x_{o,r} - x_r - dx_r)} \quad (3b)$$

$$dz = \frac{(l_{o,l} \cdot l_{o,r})(dx_l - dx_r)}{(x_{o,r} - dx_r - x_r)l_{o,l} + (x_{o,l} + dx_l + x_l)l_{o,r}} \quad (3c)$$

In the actual implementation of these equations, the MTV image pairs from each detector are first spatially correlated, as in the planar version of MTV, to establish the initial and final coordinates of the tagged regions on the detector's image plane. These coordinates are mapped onto the real object plane, using Eqs. (1) and (2), to determine the corresponding apparent in-plane coordinates. The resulting initial coordinate and displacement ( $x$ ,  $dx$ ,  $y$ ,  $dy$ ) for each tagged region from the left and right detectors are used in Eq. (3) to yield the final data.

To use the equations above, three physical parameters must be determined. These parameters are the image magnification,  $m$ , the camera viewing angle,  $\phi$ , and the distance between the image and the object plane,  $h_o$ ; see Fig. 2. It is also recognized that these relations are strictly valid when imaging through a medium with a uniform index of refraction. Viewing through media with different refractive indices, such as the air-water interface commonly encountered in laboratories, can make the three parameters mentioned above spatially non-uniform. The situation becomes even more complicated if viewing through a curved surface is required. A method of addressing the variable index of refraction with flat surfaces using ray tracing has been discussed by Prasad and Adrian (1993). For more complex imaging conditions, the use of ray-tracing approaches can be bypassed in favor of a general mapping function (Lawson and Wu 1997b; Solof et al. 1997; Willert 1997).

The approach we have taken in this study is to still use the equations we have described above and determine an "effective" set of three imaging parameters. As will be shown later, the errors introduced by this method are sufficiently small for the studies described here which involve imaging through flat air-Plexiglas-water interfaces. The calibration method for determining the "effective" imaging parameters is essentially using Eqs. (1) and (2) in reverse, along with a set of known coordinates on the object plane (i.e., target placed in the measurement region). The three imaging parameters determined in this manner are not the physical geometric parameters in the actual setup of the cameras but an effective set of parameters that takes into account the effects connected to viewing through regions with different indices of refraction.

### 3 Performance characteristics

Before discussing the tested performance characteristics of the stereo MTV system just described, it is instructive to first consider the sensitivity of the system to the various parameters. The primary conclusions of a sensitivity analysis of Eqs. (1)–(3) are as follows. In the remapping process [i.e., Eqs. (1) and (2)], it is found that among the three imaging parameters the most important is the magnification  $m$ . Furthermore, the uncertainty in  $m$  results in an uncertainty in the remapped coordinates that is not uniform over the entire image; the outer regions of the image are much more sensitive than the middle regions. It is also found that the uncertainty in the displaced pixel coordinates  $x''$  and  $y''$  (e.g., as dictated by the accuracy considerations of the correlation procedure in Gendrich and Koochesfahani 1996) maps into approximately the same uncertainty level in the remapped coordinates  $x$  and  $y$ , and this uncertainty is nearly uniform over the image.

The main conclusions from the sensitivity analysis of Eq. (3) are illustrated in Fig. 3. The uncertainty in the apparent in-plane displacements  $dx_{l,r}$  and  $dy_{l,r}$  lead to

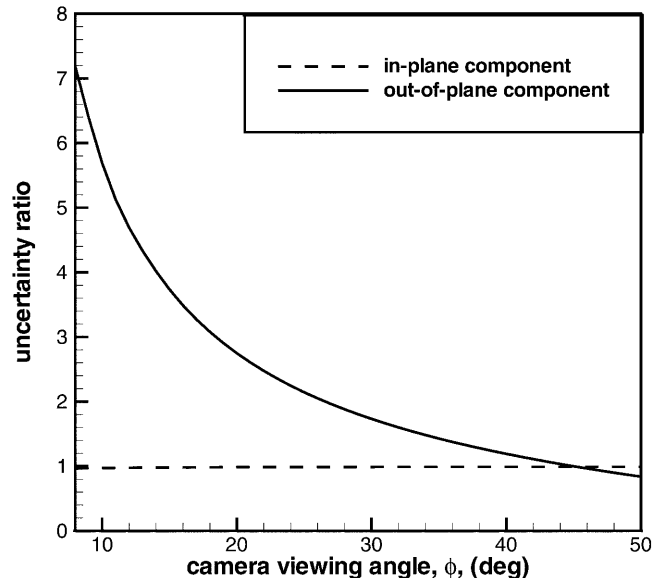


Fig. 3. Uncertainty ratio as a function of camera angle,  $\phi$ . Uncertainty ratio is defined as the ratio of the uncertainty in the actual displacements ( $dx$ ,  $dy$  or  $dz$ ) from Eq. (3) divided by the input displacement uncertainty attributed to ( $dx_l$ ,  $dx_r$ ,  $dy_l$ , or  $dy_r$ ).

about the same level of uncertainty in the actual displacements  $dx$  and  $dy$ , nearly independent of viewing angle  $\phi$ . However, the corresponding uncertainty in the actual out-of-plane displacement  $dz$  does depend on angle  $\phi$ . The information in this figure is similar to that given in Lawson and Wu (1997a), except that in Lawson and Wu the ratio of out-of-plane to in-plane uncertainty were reported (i.e., the ratio of the two curves in Fig. 3). Further, their analysis was carried out only for the central portion of the image. The current analysis shows that the trends shown in Fig. 3 are nearly the same over the entire image. We note that the viewing angle  $\phi$  can vary between 45 and 15°, depending on the experiment; imaging through air-Plexiglas-water interfaces can sometimes require angles as low as 15°. According to Fig. 3, the expected uncertainty in the actual  $dz$  displacement can be one to three times the corresponding apparent in-plane displacement uncertainty, whereas the actual in-plane displacement uncertainty remains unchanged. Therefore, a 0.05-pixel uncertainty (rms level) in determining the displacements in the planar MTV (see Gendrich and Koochesfahani 1996) results in an uncertainty of 0.05 pixel for the in-plane measurements and a 0.05–0.15 pixel in the out-of-plane component.

To assess the performance of the procedures described earlier, a series of target tests were performed. A grid target was translated at known distances, and the errors between the measured and actual displacements were quantified at all grid intersections. In tests performed in air, where Eqs. (1)–(3) are strictly valid, the camera angles were nominally at 45° and  $x$ ,  $y$ ,  $z$  displacements of up to 15 pixels (about 1.5 mm) were considered in various combinations. It was found that the measured mean displacement was within 2% of the actual value, and uniform over the image. This discrepancy is accounted for by 0.5° misalignment between the optical axis of the optics and the translational stage. Among the various trials, 90% of the rms levels were found to be less than 0.04 pixel. The rms values were uniform across the image and the levels were comparable for all three displacement components, as expected for a 45° viewing angle.

Target tests were also carried out for a typical case involving viewing through regions with different refractive indices, where Eqs. (1)–(3) are not strictly valid with a fixed set of imaging parameters. The test considered the movement of the target in a water tunnel where the cameras had to image through 30 cm of water, 2.5 cm of Plexiglas, and about 15 cm of air. The useful field of view was about 9 cm in the water tunnel and  $x$ ,  $z$  target displacements of up to 10 pixels (nearly 2 mm) were considered. The effective imaging parameters were determined as described in Sect. 2, and the effective viewing angle was determined to be 20°. Results show that the rms levels for the in-plane ( $x$ ,  $y$ ) displacements were less 0.04 pixel, similar to the air tests. The rms in the out-of-plane  $z$  displacement was at a higher value of about 0.06 pixel. These rms levels were nearly uniform across the image. In this case, however, a difference between the measured *mean*  $x$ -displacement and the actual value was noted; see Fig. 4. This error in the  $x$ -displacement was non-uniform over the image with about a  $\pm 1\%$  peak-peak spatial variation. This is a systematic variation connected

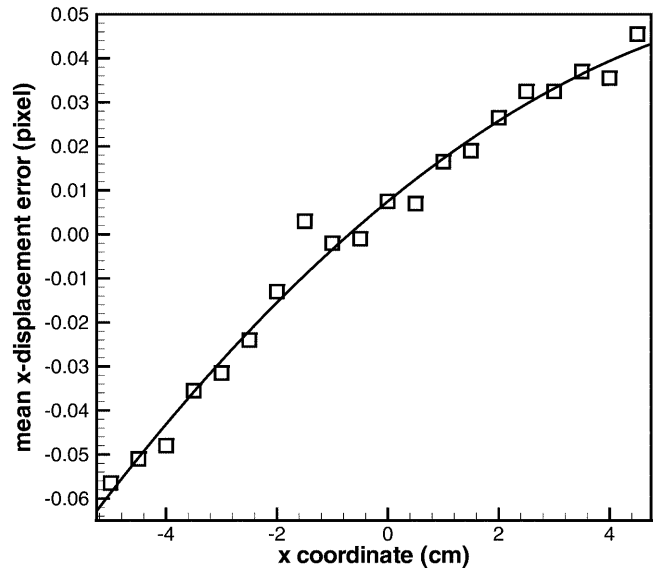


Fig. 4. Systematic variation of the mean  $x$ -displacement error across the imaged region while viewing through flat air-Plexiglas-water interfaces (see text for specific details). Data are shown for target displacement of 5 pixel. Solid curve represents the least-squares second-order fit to data

to the use of Eqs. (1)–(3) with a spatially uniform set of imaging parameters and can, in principle, be taken into account. For the results just described, and 5 pixel mean displacement, the indicated spatial variation corresponds to a maximum of 0.05 pixel. We note that the corresponding error in the mean  $z$ -displacement was much weaker (within 0.02 pixel). For the measurements currently in progress in this laboratory, these mean errors represent the worst case scenario, are considered acceptable and, if needed, can be accounted for.

#### 4

#### Results of experimental validation

The flow under a rotating disk was selected for the experimental validation of the stereo MTV technique. The setup shown in Fig. 5 illustrates a rotating flat disk (radius  $R = 6.35$  cm) inside a container of square cross section with dimensions of  $14 \times 14 \times 15.25$  cm. A DC motor is used to rotate the disk at 250 rpm ( $\pm 1$  rpm) for all experiments. The rotating disk is located 3.2 cm (0.5R) above the bottom fixed wall. The region of the flow imaged here is characterized by primarily an azimuthal flow (maximum  $V_\theta$  about 16 cm/s) and a weaker secondary flow ( $V_r$  and  $V_y$  typically five times smaller). The imaged region for three-component measurements is in the ( $r$ - $y$ ) plane and is approximately 3.5 (in  $r$ )  $\times$  2.5 cm (in  $y$ ), starting about 0.15 cm below the disk (outside the Ekman boundary layer).

The MTV measurements reported here take advantage of a phosphorescent triplex molecular complex that is premixed in water as the working fluid. The molar concentrations of the components used are  $2 \times 10^{-4}$  M  $\beta$ -cyclodextrin, 0.06 M cyclohexanol, and a saturated solution of 1-bromonaphthalene (approx.  $1 \times 10^{-5}$  M). A grid of intersecting laser lines is used for

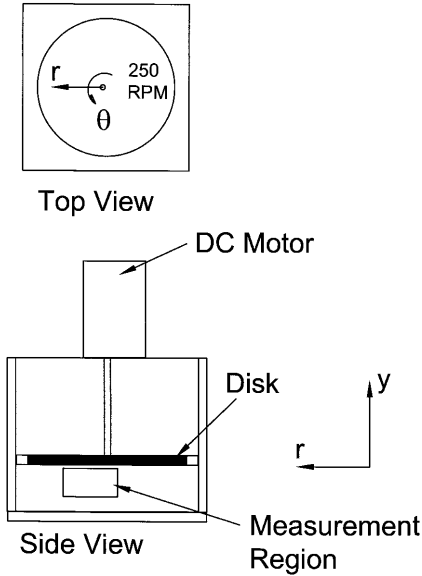


Fig. 5. Schematic of the rotating disk experiment

tagging, similar to that shown in Fig. 1. The grid is created from the beam of a Lambda Physik LPX 210i XeCl excimer laser which generates 20 ns long pulses at a wavelength of 308 nm. The number of grid intersections in this study was about 350. The tagged regions are imaged on Pulnix TM9701 CCD (30 frame/s) cameras, whose output are acquired and transferred to disk in real time using PC-based image acquisition systems. Additional details of the experimental procedure, optics, and the spatial correlation method used for estimating the displacement vector can be found in Gendrich and Koochesfahani (1996) and Gendrich et al. (1997).

To evaluate the performance of the stereo MTV technique, reliable reference velocity data are needed. The baseline reference data for this flow were obtained from the measurement of the  $(V_\theta, V_r)$  velocity components over the  $(r-\theta)$  plane at a given  $y$  distance away from the disk using standard two-component MTV with viewing through the bottom of the test section. Because the out-of-plane velocity component (i.e.,  $V_y$  in this case) is very small, accurate measurements of the in-plane velocity components  $V_\theta, V_r$  can be made and used for comparison. The stereoscopic measurements were made of the three components of the velocity over the  $(r-y)$  plane as shown in Fig. 5. In this case, the out-of-plane velocity component  $V_\theta$  is much larger (by about a factor of 5) compared with the other two components. The approach just described allows the comparison of velocity data  $(V_\theta, V_r)$  between the stereo method and the measured reference data along the radial line defining the intersection of the two measurement planes. Since the two measurements were not carried out simultaneously, comparisons cannot be provided on the basis of the instantaneous velocity data. Instead, we compare the mean and rms fluctuation of the velocity data computed from 7200 realizations. The comparison of the mean and rms profiles of the primary velocity component  $V_\theta$  is illustrated in Fig. 6. We note the excellent agreement between the profiles measured by the

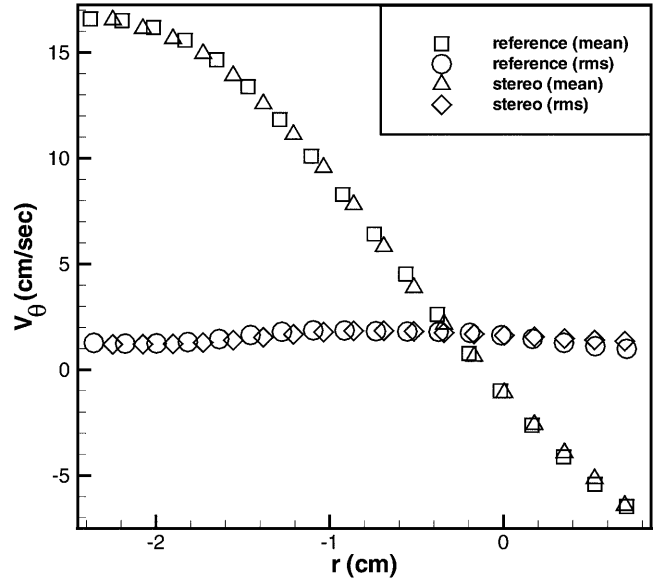


Fig. 6. Comparison of  $V_\theta$  from stereoscopic MTV with planar reference MTV data. Data at  $y = -0.43$  cm

stereo method and the reference data. The maximum out-of-plane speed of 16 cm/s in Fig. 6 would correspond to a  $z$  displacement of a tagged region of about 0.8 mm. It should be mentioned that the effects of the nonuniform systematic mean error discussed in Sect. 3 are much reduced in this experimental setup because the thickness of the container wall and the depth of water imaged through are much smaller than those used in the target tests.

Figure 7 shows the mean velocity field over the entire measurement plane determined from stereo MTV. It is noted that the mean flow is not symmetric. The mean features of the secondary flow show an asymmetric recirculation pattern. The out-of-plane, azimuthal, velocity component, shown as a shaded contour plot, is zero near the center of the disk, and increases towards the outer edge

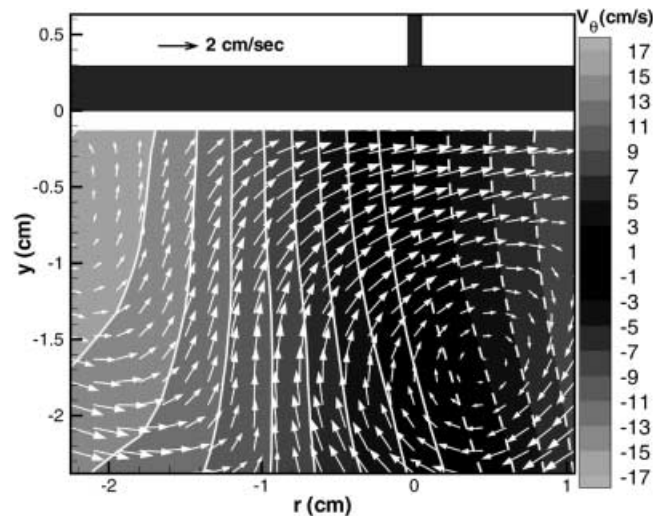


Fig. 7. Complete mean velocity field in the  $(r-y)$  plane for the rotating disk. Out-of-plane velocity ( $V_\theta$ ) is indicated by flooded and line contours. Dashed lines indicate negative velocity

of the disk, as expected. Note that the azimuthal velocity is not a linear function of  $r$  and also exhibits a slight asymmetry.

### 5 Example of application to a highly unsteady vortical flow

In this section, we show three-component velocity data for a highly three-dimensional flow field where the instantaneous velocity components are comparable in magnitude. The flow is generated by a model propeller rotating at 250 rpm inside a closed container; see the schematic in Fig. 8. There is no external flow moving past the propeller except for the flow generated by the propeller itself. The imaged region is approximately  $3 \times 3$  cm. An example of the instantaneous velocity field ( $V_r, V_\theta, V_y$ ) and the corresponding mean velocity field, as well as the azimuthal vorticity component ( $\omega_\theta$ ) are provided in Fig. 9. It is important to note that the highest level of out-of-plane velocity (i.e.,  $V_\theta$ ) occurs in a well-defined region nearly at the same location as the (negative) peak of azimuthal vorticity. This observation was generally true for all the instantaneous realizations recorded. The mean velocity field clearly shows the predominant downward flow generated by the propeller. Note that the mean value of the azimuthal vorticity is much reduced compared with its instantaneous peak levels.

### 6 Conclusions

A stereoscopic molecular tagging velocimetry (sMTV) technique has been described which extends the capabilities of MTV to provide instantaneous three-component measurements over a plane. This technique is based on the angular displacement method. Sensitivity analysis indicates that over the range of configurations typically expected in MTV experiments the in-plane velocity components will have nominally the same level of error as would be expected from the base two-component MTV technique. The error in the out-of-plane velocity component can be one to three times larger than the in-plane error level, depending upon the camera configuration.

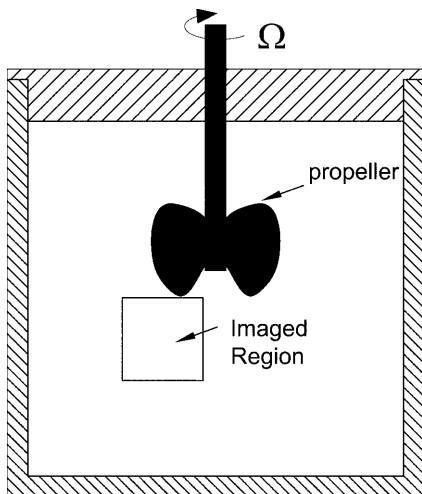


Fig. 8. Schematic of model boat propeller and the imaged region

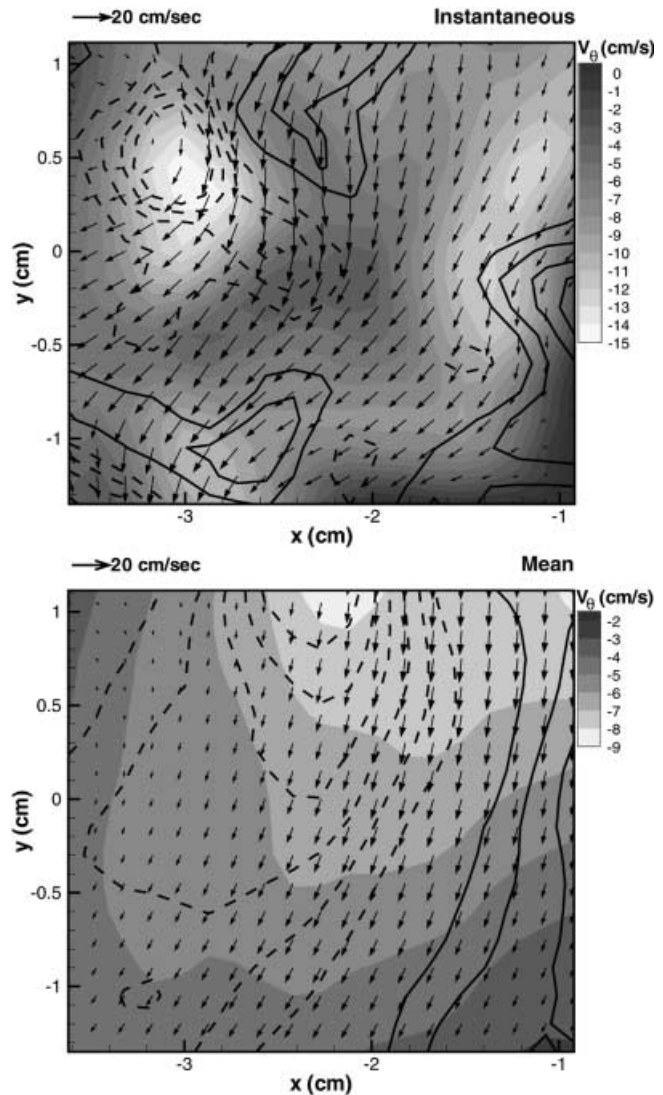


Fig. 9. Instantaneous and mean velocity and  $\omega_\theta$  fields under a model boat propeller. Out-of-plane velocity ( $V_\theta$ ) is indicated by flooded contours. Vorticity is indicated by line contours. Dashed lines indicate negative vorticity. Contour levels are: instantaneous [ $\omega_\theta = \pm 10, \pm 20, \dots$  ( $s^{-1}$ )]; mean [ $\omega_\theta = \pm 2, \pm 4, \dots$  ( $s^{-1}$ )]

ration. A technique for the calculation of the calibration parameters from a reference target image is developed, and shown to lead to results with acceptable error levels even while imaging through regions of varying indices of refraction. The resulting spatial non-uniformity that develops in this case produces a systematic source of error that can be accounted for, if necessary. The performance of the stereoscopic MTV technique have been confirmed by comparing experimental results in the flow field of a rotating disk inside a container. The application of the technique is also demonstrated in the flow field of a rotating model boat propeller, where the instantaneous velocity components are comparable in magnitude.

### References

Arroyo MP; Greated CA (1991) Stereoscopic particle image velocimetry. Meas Sci Technol 2: 1181-1186

- Gauthier V; Riethmuller ML** (1988) Application of DPIV to complex flows: measurements of the third component. Von Karman Institute for Fluid Dynamics, Lecture Series 1988-06
- Gendrich CP; Koochesfahani MM** (1996) A spatial correlation technique for estimating velocity fields using molecular tagging velocimetry (MTV). *Exp Fluids* 22: 67-77
- Gendrich CP; Koochesfahani MM; Nocera DG** (1997) Molecular tagging velocimetry and other novel applications of a new phosphorescent supramolecule. *Exp Fluids* 23: 361-372
- Hill DF; Sharp KV; Adrian RJ** (1999) Distortion compensation applied to stereoscopic PIV in a mixing tank. Proceedings of the 3rd ASME/JSME Joint Fluids Engineering Conference, FEDSM 99-7265, 19-23 July
- Koochesfahani MM** (1999) Molecular tagging velocimetry (MTV): progress and applications. 30th AIAA Fluid Dynamics Conference, AIAA Paper 99-3786, 28 June-1 July, Norfolk, Va.
- Koochesfahani MM; Cohn RK; Gendrich CP; Nocera DG** (1996) Molecular tagging diagnostics for the study of kinematics and mixing in liquid phase flows. Proceedings of the Eight International Symposium on Applications of Laser Techniques to Fluids Mechanics, July 8-11, 1996, Lisbon, Portugal, vol. I, 1.2.1-1.2.12; Also in *Developments in Laser Techniques and Fluid Mechanics*, Chapter 2, section 1, Eds. Adrian, Durao, Durst, Maeda, Whitelaw. Springer-Verlag, 1997
- Lawson NJ; Wu J** (1997a) Three dimensional particle image velocimetry: error analysis of stereoscopic techniques. *Meas Sci Technol* 8: 894-900
- Lawson NJ; Wu J** (1997b) Three dimensional particle image velocimetry: experimental error analysis of a digital angular stereoscopic system. *Meas Sci Technol* 8: 1455-1464
- Prasad AK; Adrian RJ** (1993) Stereoscopic particle image velocimetry applied to fluid flows. *Exp Fluids* 15: 49-60
- Solof SM; Adrian RJ; Liu ZC** (1997) Distortion compensation for generalized stereoscopic particle image velocimetry. *Meas Sci Technol* 8: 1441-1454
- von Oord J** (1997) The design of a stereoscopic DPIV system. Delft University Technical Report MEAH-161
- Westerweel J; Nieuwstadt FT** (1991) Performance tests on 3-dimensional velocity measurements with a two camera digital particle image velocimeter. *Laser Anemometry* 1: 349-355
- Willert C** (1997) Stereoscopic digital particle image velocimetry for application in wind tunnel flows. *Meas Sci Technol* 8: 1465-1479